

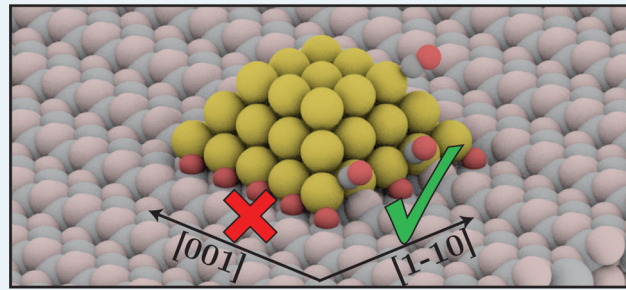
Identification of the Catalytic Site at the Interface Perimeter of Au Clusters on Rutile TiO₂(110)

Lasse B. Vilhelmsen and Bjørk Hammer*

Interdisciplinary Nanoscience Center (iNANO) and Department of Physics and Astronomy, Aarhus University, DK-8000 Aarhus C, Denmark

 [Supporting Information](#)

ABSTRACT: We present a density functional theory study of the CO oxidation reaction at a Au₂₄ cluster supported on a rutile TiO₂(110) slab. The global minimum structure of the Au₂₄ cluster is found using a genetic algorithm search. Catalytic sites are found at the perimeter of the Au–TiO₂ interface but with strong dependence on the surface direction. It is shown how the CO oxidation reaction only happens along the [1̄10] direction of the support and not along the [001] direction. This effect is attributed to a too weak CO binding energy along the [001] direction caused by the charge state and Au–Au coordination of the Au atoms along this direction.



KEYWORDS: gold, heterogeneous catalysis, density functional theory, global optimization, TiO₂, CO oxidation

INTRODUCTION

Supported gold nanoparticles have been extensively investigated for a number of catalytic applications since the discovery in the late eighties of nanometric gold's high catalytic activity.^{1–6} Gold clusters show great promise in hydrogen purification for fuel cells, synthesis of fine chemicals, and for a number of organic reactions.^{7,8} The most studied reaction on supported Au clusters is probably the CO oxidation reaction.^{3,5,9–12} This seemingly simple reaction is effectively catalyzed by Au clusters supported on a reducible oxide like rutile TiO₂, but the full atomic understanding of the active site remains elusive.

Many studies during the past decade have established experimentally^{2,3,13–15} and through the support of theory^{16–18} that the active site for CO oxidation is at the perimeter between the TiO₂ support and the Au cluster. Some studies show that O₂ is adsorbed and activated in a dual-catalytic site coordinating to both Ti in the support and Au at the cluster,^{18,19} whereas other studies propose that O₂ is directly activated at the Au structure.^{20,21} Although the O₂ activation is debated, there is a consensus that CO is supplied through adsorption and diffusion either along the Ti trough of the support or from low-coordinated Au atoms at the cluster.

Although the overall reaction mechanism has been established, it remains a challenge to determine which properties of the catalyst controls the catalytic activity. From a geometrical point of view, the governing factors are under-coordinated Au atoms,²² the structural fluxionality of the Au clusters,^{23,24} and the presence of specific sites at the perimeter between the support and the Au cluster.^{3,18} From an electronic point of view, the governing factors are the presence of loosely bound excess electrons from reducing defects in the oxide²⁵

and the charge state of the Au atoms.^{26,27} It is now believed that it is a positive interplay between several of these properties that enhances the catalytic activity. To operate optimally, the catalyst thus needs to have both the correct local atomic geometry and available charge such that the O₂ molecule can be activated and the CO molecule can react with the O.

In a recent paper, we theoretically described the high thermal stability of interfacial oxygen between supported Au clusters and the TiO₂ support,²⁷ which conforms with experimental observations of nanosized Au oxide structures.^{28–31} The O atoms at the interface adsorb on top the 5-fold coordinated Ti atoms (5f-Ti) at the surface and thus coordinate to both Au and Ti atoms simultaneously. This interfacial oxygen is stabilized by reducing defects in the support, but it is stable regardless of crystal reduction. One effect of this oxide layer is that all Au atoms at the perimeter along the [001] direction of the substrate are cationic. Because of this cationicity and the predicted high Au–Au coordination of the Au atoms along this direction, it was shown how the perimeter along the [001] direction of the support does not contribute significantly to the catalytic activity.

The specific aim of this study is to establish the catalytic activity of the [1̄10] perimeter direction compared to the [001] one. As the [1̄10] direction is perpendicular to the [001] direction, we can simultaneously investigate the properties of the two by employing a sufficiently large cluster model. We choose to investigate a Au₂₄ cluster, because it is large enough to contain significant amounts of both directions while at the

Received: February 14, 2014

Revised: April 4, 2014

Published: April 11, 2014



same time being within a size range (≈ 1 nm) tractable on current computational hardware.

After a description of the relevant methods in the Computational Details, a detailed determination of the atomic structure of the Au_{24} cluster adsorbed on a preoxidized surface is discussed. Then the adsorption of CO is considered and understood in terms of the charge state and coordination of the Au cluster, and lastly, full catalytic cycles are determined both along the $[1\bar{1}0]$ direction and at the corner between the two directions. The results of this analysis are compared to previous results for the CO oxidation reaction along the $[001]$ direction and finally CO coverage effects are discussed.

COMPUTATIONAL DETAILS

All calculations were performed using the grid-based projector augmented wave (GPAW) program.^{32,33} The structural searches were done on a two trilayer thick $\text{TiO}_2(110)$ slab together with the PBE functional³⁴ using a linear combination of atomic orbitals (LCAO) d_{z^2} -basis.³⁵ For the calculation of binding and reaction energies, a four trilayer thick slab is used together with the M06-L functional^{36,37} and a real space grid basis with a grid spacing of approximately 0.18 Å. Reaction barriers are established using the climbing image–nudged elastic band (CI–NEB) method.³⁸ Due to the size of the supercell, only a two trilayer thick slab is used for these calculations. It has been verified that only small changes in the binding energies exist using this thinner slab and that the reaction energies only change by a similar magnitude when probing the well characterized odd–even effect with respect to the number of TiO_2 trilayers^{39,40} (see Figure S1). For all calculations, the only k -point considered is the Γ -point and no ZPE energy contributions will be included.

All energetics presented in this paper are calculated using the M06-L functional. This functional is used due to its improved description of both bulk and cluster properties of Au⁴¹ and because of its precise prediction of the formation energy of O_2 (see ref 24).

The supercell used in this study is a $p(5 \times 3)$ supercell with H adsorbed at each bridging O at the back of the slab (see Figure 1a). It was established in ref 27 that reducing the TiO_2 crystal increases the stability of the interfacial oxide layer, and the degree of reduction used in this study is the same as in that study. This degree of reduction is chosen in order to mimic a TiO_2 crystal prepared under surface science conditions. The $p(5 \times 3)$ supercell is sufficiently large that a Au_{24} cluster can fit onto the surface without significant self-interaction. For all calculations, one Ti atom at the back of the slab is kept fixed.

Due to the size of the Au cluster and Au's large structural fluxionality, it is a significant challenge to reliably predict the global minimum (GM) of the Au_{24} cluster adsorbed on the surface. To solve this challenge, we employ a first-principles-based genetic algorithm (FP-GA) to establish the structure of the adsorbed clusters.^{24,42} Compared to our previous studies, the only addition made to the FP-GA method is the inclusion of a mirror mutation which mirrors a cluster through a plane randomly oriented perpendicular to the surface and positioned through the cluster's center of mass. This mutation is applied to 15% of the proposed clusters.

RESULTS AND DISCUSSION

Starting now with a determination of the global minimum structure of the Au_{24} cluster adsorbed onto the preoxidized surface. The structure of the adsorbed Au_{24} cluster is established assuming two different amounts of O preadsorbed on the surface. Figure 1b shows the predicted GM for the cluster adsorbed on a pattern of eight O atoms adsorbed on 5f-Ti sites (six of the eight atoms are visible with the remaining two directly below the cluster). Figure 1c shows the GM when 12 O atoms are preadsorbed in a 4×3 pattern on the surface. The FP-GA has tested more than 1300 structures in order to

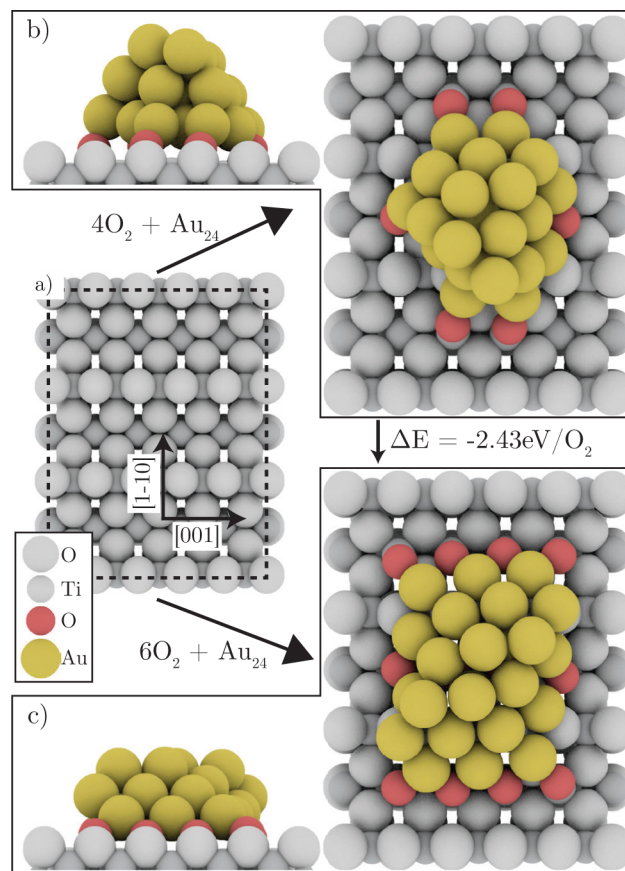


Figure 1. (a) Surface used for all studies of adsorbed Au_{24} . O atoms are drawn as large spheres and Ti atoms as small. (b) Four O_2 are preadsorbed on 5f-Ti atoms on the surface (6 O are visible in the figure with the remaining two below the Au cluster). The Au_{24} cluster is optimized on top. (c) Six O_2 are preadsorbed on 5f-Ti atoms in a 4×3 pattern. The Au_{24} cluster is optimized on top.

find the two GM structures shown in Figure 1b,c (see Figure S2 and Figure S3 for more structures). By comparing the energy of the structures in Figure 1b,c we see that the additional two O_2 molecules undergo a potential energy change of $\Delta E = -2.43 \text{ eV/O}_2$. This confirms a strong bias toward oxidizing the interface between the TiO_2 support and the Au cluster.

Comparing the two structures in Figure 1b,c shows how the Au cluster transforms from a three-layer cluster when coordinating to eight O atoms to a more flat pseudo two-layer structure when coordinating to 12 O atoms. This flattening of the Au cluster confirms the high structural fluxionality of the Au cluster; the energy gained by the additional O outweighs the cost of reducing the overall Au coordination.⁴³ A further flattening may be expected if even more O is provided; however, as the scope of this study is to investigate the edges of the Au clusters, we refrain from pursuing this.

Having determined the structure of the Au_{24} cluster adsorbed on the 4×3 O pattern, we now turn to the systematic investigation of CO adsorption. In ref 27, we established the weak adsorption of CO along the $[001]$ direction, with the most stable adsorption site close to the perimeter being a 3-fold site. This adsorption site is shown in Figure 2a,b, and it is confirmed that this site remains a weak CO adsorption site for the Au_{24} cluster. The binding energy is increased by 0.14 eV adsorbing CO at a cluster, but compared to a calculated CO

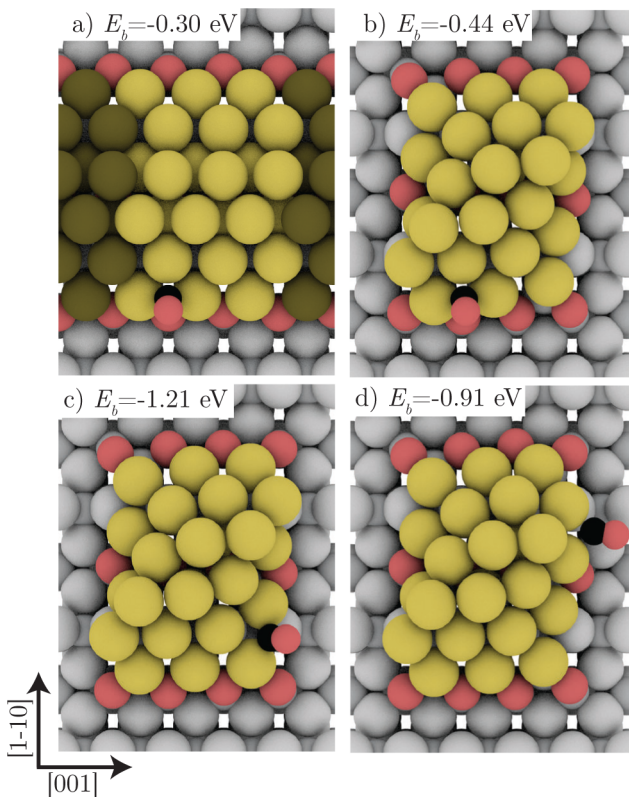


Figure 2. (a) CO adsorbed along a periodic Au rod—the structure is taken from ref 27. Twenty-four of the Au atoms are colored bright for easy comparison. (b) CO adsorbed along the [001] direction of the substrate. (c) CO adsorbed at the corner of the Au_{24} cluster. (d) CO adsorbed along the $[1\bar{1}0]$ direction of substrate. C is colored black.

adsorption potential energy of $E_b = -0.78$ eV on the top Ti atoms in the trough, it is still a weak binding site.

Figure 2c shows the overall most stable adsorption site found at the Au_{24} cluster with an adsorption potential energy of $E_b = -1.21$ eV. The adsorption site is at the corner of the Au_{24} cluster with CO coordinating to two very under-coordinated cationic Au atoms (see Figure 3). Further along the $[1\bar{1}0]$ direction, a second strong adsorption site is found with an adsorption potential energy of $E_b = -0.91$ eV. This adsorption

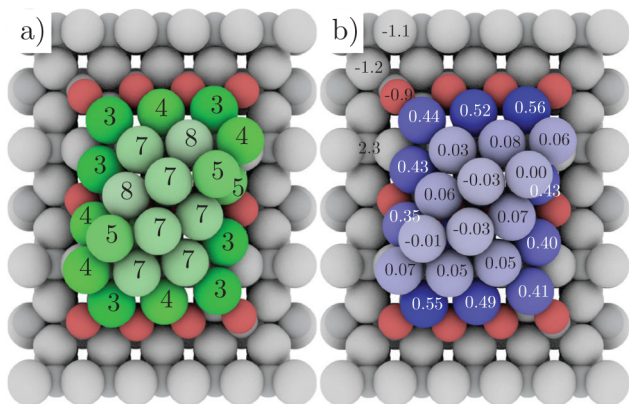


Figure 3. (a) Coordination number of each Au atom. (b) Bader charge for each Au atom. For the O and Ti atoms, the charge is shown for one unique representative of each coordination and type. The coloring of the Au atoms reflects the coordination (a) and charge state (b), respectively.

site is interesting, because it is along the $[1\bar{1}0]$ direction and not at a corner, thus confirming the presence of strong CO adsorption sites along this perimeter direction. The perimeter is interesting compared to corners, because at larger clusters the number of edge sites increases compared to the number of corner sites.⁴⁴ All tested CO adsorption sites not shown here are shown in Figure S4 of the Supporting Information.

Figure 3a shows the number of nearest Au neighbors for each Au atom and Figure 3b the Bader charge assigned to each Au atom.⁴⁵ The Bader charge analysis is in agreement with ref 27, showing that only Au atoms in direct contact with O atoms are cationic; the rest of the Au atoms are close to neutral. When comparing the CO adsorption sites in both Figure 2 and Figure S4, it is seen that our results confirm previous results showing that CO preferentially binds at low coordinated Au atoms.⁴⁶ Comparing Figure 2a and Figure 2b, it is evident how the Au cluster, even for this small cluster size, resembles the periodic close packed structure along the $[001]$ direction.²⁷ The cluster thus quickly forms a closely packed inert structure in this direction at which CO cannot bind. This however does not happen along the $[1\bar{1}0]$ direction, because the perpendicular bridging O atom rows presented here create a more open structure.

Having established the existence of strong CO adsorption sites along the $[1\bar{1}0]$ direction, we now turn to an investigation

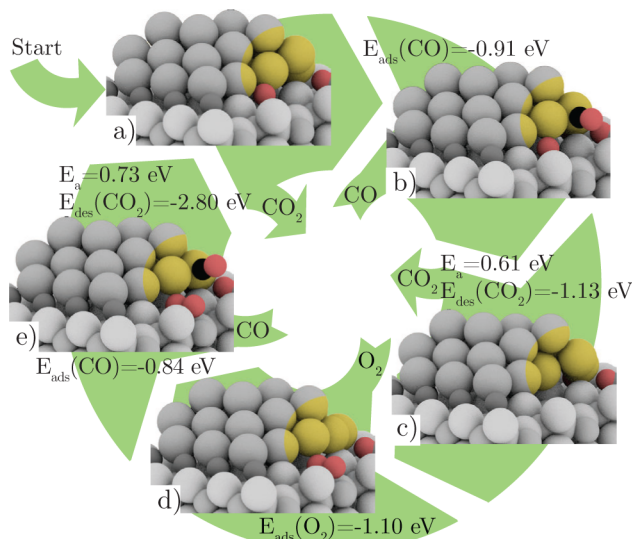


Figure 4. Full catalytic cycle for the $\text{O}_2 + 2\text{CO} \rightarrow 2\text{CO}_2$ reaction at the $[1\bar{1}0]$ edge of the Au_{24} cluster. The reaction goes via the configuration in Figure 2d. Only the relevant part of the supercell is shown in color.

of the catalytic activity along this direction. Figure 4 shows a full reaction cycle for the



reaction. The reaction starts in Figure 4a with the bare Au_{24} cluster. CO then adsorbs at the site shown in Figure 2d (Figure 4b). From there, the CO molecule moves toward the O at the perimeter and forms CO_2 which desorbs (image b to c). The activation energy for this reaction is $E_a = 0.61$ eV. In the O vacancy between the support and the Au cluster, an O_2 molecule adsorbs (images c–d), and a second CO subsequently adsorbs in the same site as the first CO (image e). To complete

the catalytic cycle, the CO molecule aids the splitting of the O₂ molecule to form CO₂ with an activation energy of $E_a = 0.73$ eV (image e to a). This last part is the step with the highest transition state energy, and the corresponding CI-NEB calculation is shown in Figure S5.

All reaction steps appearing in Figure 4 have a transition state energy below the adsorption energy of the individual reactants. In our previous study of the catalytic activity along the [001] direction, this was not the case due to the weak adsorption of CO along the [001] direction.

The reaction along the [1̄10] direction can be compared to a similar reaction at the corner of the Au₂₄ cluster. Figure 5 shows

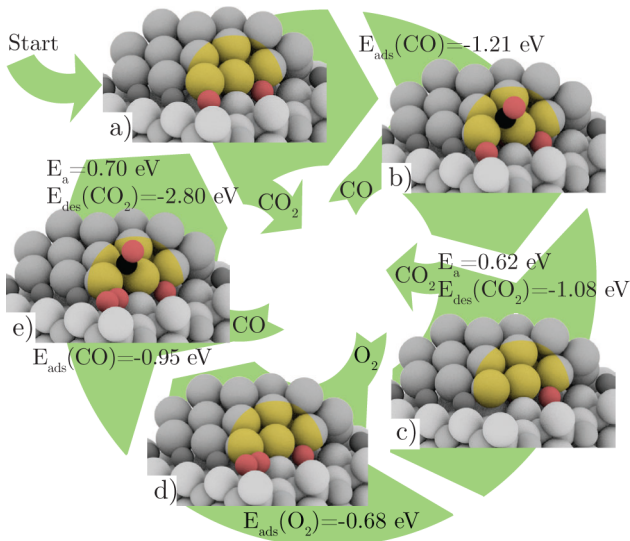


Figure 5. Full catalytic cycle for the $O_2 + 2CO \rightarrow 2CO_2$ reaction at the corner of the Au₂₄ cluster. The reaction goes via the configuration in Figure 2c.

the same reaction steps as in Figure 4 only starting from the CO molecule in Figure 2c. The activation energy for this reaction is almost the same as along the edge, again with the reaction step from image e to a being the one with the largest activation barrier. The step with the largest activation energy is the same for the two reactions, but the nature of this step is somewhat different. Figure S5b shows the transition state for the reaction along the [1̄10] direction. The barrier for this step stems from breaking the O₂ bond. For the reaction at the corner the energy barrier is instead determined by the energy cost of moving the CO molecule away from its strongly bound starting point and close to the O₂ molecule (see Figure S6).

Figure 6 summarizes the reaction steps with the largest activation barriers for the two reactions shown in Figure 4 and 5. The figure also shows the transition state with highest energy from our previous study of Au rods along the [001] direction.²⁷ The figure clearly shows how reactions along the [001] direction are prohibited because of the too weak adsorption of CO, and it also shows how both the corner and the [1̄10] direction are catalytically active. The reaction along the [1̄10] direction involves two barriers. The first barrier (dotted line) is associated with breaking the O₂ molecule, whereas the second originates from reacting CO with O. At the corner, the CO molecule can react directly with the O₂ species, and there the barrier is instead associated with moving the CO molecule away from a very stable starting point.

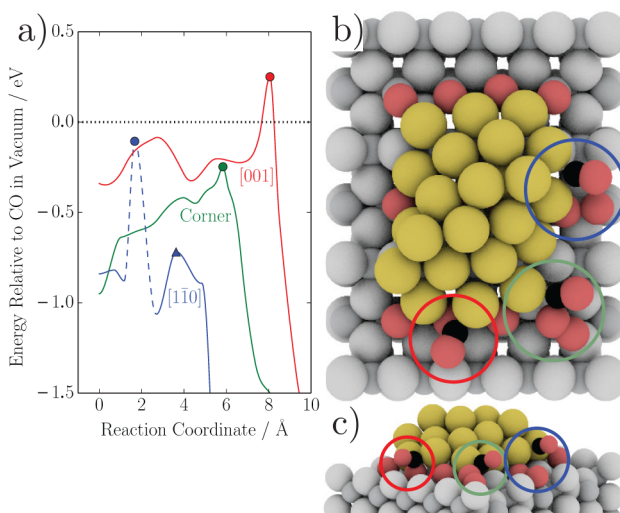


Figure 6. Summary of the reaction steps with the highest activation barriers for each catalytic cycle investigated. The reactions along the [1̄10] direction and at the corner are detailed in Figures 4 and 5, whereas the reaction along the [001] direction is described in ref 27. The graph in (a) shows the energetics along the path and the drawings in (b) (c) schematically show the transition states marked with a filled disk in (a). The dashed part of the blue line indicates an O₂ dissociation, whereas the other transition states stems from CO reacting with the O atom ([001]) or with the O₂ molecule (corner). The point annotated with a triangle in (a) is shown in Figure S5b.

The Au cluster model explored in the present work differs from previous studies of the Au/TiO₂ catalyst because we employ a global minimum structure for Au and because we completely oxidize the interface between the cluster and the support.^{3,16,18,19,47,48} The reaction cycles found here do however have many similarities to the ones described in the literature. Some studies start from CO at the cluster,^{16,18,47,48} but others propose that CO is supplied from the support.^{3,19} If in our work CO is supplied from the trough, the activation energy changes to $E_a = 0.79$ eV, compared to the $E_a = 0.61$ eV in Figure 4, for the reaction along the [1̄10] direction. This shows that the activation barriers for the two processes are fairly close but subject to change if the support structure and reduction conditions are modified. For the CO oxidation reaction at the corner (Figure 5), we predict that CO reacts directly with the activated O₂ complex, which is also the case in refs 3, 16, 18, 19, 47. Along the [1̄10] direction, however, we calculate that it is favored to dissociate the O₂ molecule before reacting it with CO. This is because the O atom between the Au₂₄ cluster and the support gains a significant amount of energy by being in its optimal position.

A highest activation energy of $E_a \approx 0.7$ eV seems high compared to the observed experimental activation energies reported in the literature of 0.16 eV to 0.59 eV for the CO oxidation reaction at Au clusters on TiO₂(110).^{3,12,19,49,50} There are several reasons for this: First, the employed model is based on a global minimum structure which is inherently very stable and thus less reactive than higher energy structures.⁴⁷ Second, Au's structural fluxionality, which has been shown to reduce reaction barriers, is not considered.⁵¹ Lastly, CO coverage effects are not included even though results for CO on Pt show an exponential dependence of the CO adsorption energy with coverage.⁵²

To probe coverage effects, we simultaneously adsorb a CO molecule on each corner of the cluster, as shown in Figure S7. The adsorption energies are calculated by removing one CO molecule at a time, and they turn out to be reduced by only 0.04 to 0.09 eV, compared to having one CO adsorbed at a time. The adsorption energy is still well above the adsorption energy of CO in the trough, which shows that the cluster will be covered by significant amounts of CO before CO covers the TiO₂ surface. Because of the reduced CO adsorption energy, it is likely that the reaction barrier for the reaction at corner sites will be reduced by at least 0.05 eV if coverage effects are taken into account and possibly by a higher value if the cluster is covered by even more CO packed closer together.

CONCLUSION

In this article, we have investigated the consequences of O on top and 5f-Ti atoms below TiO₂(110)-supported Au clusters. Such interfacial oxygen is stabilized by reducing defects in the substrate and by charge transfer from the adsorbed Au cluster.²⁷ By using the global minimum Au₂₄ structure, we predict the presence of CO at the Au cluster along the [1̄10] direction of the substrate while the [001] direction remains void of CO. Both the [1̄10] direction and the corner of the Au₂₄ cluster are predicted to catalyze the CO oxidation reaction with an activation energy of 0.7 eV. Lastly, it is predicted that an increased CO coverage will reduce this barrier by at least 0.05 eV at corner sites.

ASSOCIATED CONTENT

Supporting Information

TiO₂ layer dependence analysis, additional structures of Au₂₄ as found with the GA, details of all CO adsorption sites investigated, additional information about the reaction paths shown in Figure 6, and details about CO coverage effects. This material is available free of charge via the Internet at <http://pubs.acs.org>.

AUTHOR INFORMATION

Corresponding Author

*E-mail: hammer@phys.au.dk.

Notes

The authors declare no competing financial interest.

ACKNOWLEDGMENTS

This work received support from the Lundbeck Foundation, The Danish Council for Independent Research, COST action CM1104, Nordforsk, and the Danish Center for Scientific Computing.

REFERENCES

- (1) Haruta, M. *Catal. Today* **1997**, *36*, 153–166.
- (2) Haruta, M. *CATTECH* **2002**, *6*, 102–115.
- (3) Green, I. X.; Tang, W.; Neurock, M.; Yates, J. T. *Science* **2011**, *333*, 736–739.
- (4) Cuenya, B. R. *Thin Solid Films* **2010**, *518*, 3127–3150.
- (5) Min, B. K.; Friend, C. M. *Chem. Rev.* **2007**, *107*, 2709–2724.
- (6) Chen, M.; Goodman, D. W. *Chem. Soc. Rev.* **2008**, *37*, 1860–1870.
- (7) Bond, G. C.; Thompson, D. T. *Catal. Rev.: Sci. Eng.* **1999**, *41*, 319–388.
- (8) Hashmi, A. S. K.; Hutchings, G. J. *Angew. Chem., Int. Ed.* **2006**, *45*, 7896–7936.
- (9) Chen, M.; Goodman, D. W. *Acc. Chem. Res.* **2006**, *39*, 739–746.
- (10) Saint-Lager, M.-C.; Laoufi, I.; Bailly, A. *Faraday Discuss.* **2013**, *162*, 179–190.
- (11) Lira, E.; Hansen, J. Ø.; Merte, L. R.; Sprunger, P. T.; Li, Z.; Besenbacher, F.; Wendt, S. *Top. Catal.* **2013**, *56*, 1460–1476.
- (12) Maeda, Y.; Iizuka, Y.; Kohyama, M. *J. Am. Chem. Soc.* **2012**, *135*, 906–909.
- (13) Kuwauchi, Y.; Yoshida, H.; Akita, T.; Haruta, M.; Takeda, S. *Angew. Chem., Int. Ed.* **2012**, *51*, 7729–7733.
- (14) Kotobuki, M.; Leppelt, R.; Hansgen, D. A.; Widmann, D.; Behm, R. J. *J. Catal.* **2009**, *264*, 67–76.
- (15) Widmann, D.; Behm, R. J. *Angew. Chem., Int. Ed.* **2011**, *50*, 10241–10245.
- (16) Liu, Z.-P.; Gong, X.-Q.; Kohanoff, J.; Sanchez, C.; Hu, P. *Phys. Rev. Lett.* **2003**, *91*, 266102.
- (17) Laursen, S.; Linic, S. *Phys. Chem. Chem. Phys.* **2009**, *11*, 11006–11012.
- (18) Molina, L. M.; Rasmussen, M. D.; Hammer, B. *J. Chem. Phys.* **2004**, *120*, 7673–7680.
- (19) Green, I. X.; Tang, W.; McEntee, M.; Neurock, M.; Yates, J. T. *J. Am. Chem. Soc.* **2012**, *134*, 12717–12723.
- (20) Sun, K.; Kohyama, M.; Tanaka, S.; Takeda, S. *ChemCatChem* **2013**, *5*, 2217–2222.
- (21) Iizuka, Y.; Tode, T.; Takao, T.; Yatsu, K.; Takeuchi, T.; Tsubota, S.; Haruta, M. *J. Catal.* **1999**, *187*, 50–58.
- (22) Xu, Y.; Mavrikakis, M. *J. Phys. Chem. B* **2003**, *107*, 9298–9307.
- (23) Häkkinen, H.; Abbet, S.; Sanchez, A.; Heiz, U.; Landman, U. *Angew. Chem., Int. Ed.* **2003**, *42*, 1297–1300.
- (24) Vilhelmsen, L. B.; Hammer, B. *Phys. Rev. Lett.* **2012**, *108*, 126101.
- (25) Madsen, G. K. H.; Hammer, B. *J. Chem. Phys.* **2009**, *130*, 044704.
- (26) Hong, S.; Rahman, T. S. *J. Am. Chem. Soc.* **2013**, *135*, 7629–7635.
- (27) Vilhelmsen, L. B.; Hammer, B. *J. Chem. Phys.* **2013**, *139*, 204701.
- (28) Dumbuya, K.; Cabailh, G.; Lazzari, R.; Jupille, J.; Ringel, L.; Pistor, M.; Lytken, O.; Steinrück, H. P.; Gottfried, J. M. *Catal. Today* **2012**, *181*, 20–25.
- (29) van Bokhoven, J. A.; Louis, C.; Miller, J. T.; Tromp, M.; Safonova, O. V.; Glatzel, P. *Angew. Chem., Int. Ed.* **2006**, *45*, 4651–4654.
- (30) Ono, L. K.; Cuenya, B. R. *J. Phys. Chem. C* **2008**, *112*, 4676–4686.
- (31) Fu, L.; Wu, N. Q.; Yang, J. H.; Qu, F.; Johnson, D. L.; Kung, M. C.; Kung, H. H.; Dravid, V. P. *J. Phys. Chem. B* **2005**, *109*, 3704–3706.
- (32) Enkovaara, J.; Rostgaard, C.; Mortensen, J. J.; Chen, J.; Dulak, M.; Ferrighi, L.; Gavnholm, J.; Glinsvad, C.; Haikola, V.; Hansen, H. A.; Kristoffersen, H. H.; Kuusima, M.; Larsen, A. H.; Lehtovaara, L.; Ljungberg, M.; Lopez-Acevedo, O.; Moses, P. G.; Ojanen, J.; Olsen, T.; Petzold, V.; Romero, N. A.; Stausholm-Møller, J.; Strange, M.; Tritsaris, G. A.; Vanin, M.; Walter, M.; Hammer, B.; Häkkinen, H.; Madsen, G. K. H.; Nieminen, R. M.; Nørskov, J. K.; Puska, M.; Rantala, T. T.; Schiøtz, J.; Thygesen, K. S.; Jacobsen, K. W. *J. Phys.: Condens. Matter* **2010**, *22*, 253202.
- (33) Mortensen, J.; Hansen, L.; Jacobsen, K. *Phys. Rev. B* **2005**, *71*, 035109.
- (34) Perdew, J. P.; Burke, K.; Ernzerhof, M. *Phys. Rev. Lett.* **1996**, *77*, 3865–3868.
- (35) Larsen, A. H.; Vanin, M.; Mortensen, J. J.; Thygesen, K. S.; Jacobsen, K. W. *Phys. Rev. B* **2009**, *80*, 195112.
- (36) Zhao, Y.; Truhlar, D. G. *J. Chem. Phys.* **2006**, *125*, 194101.
- (37) Ferrighi, L.; Madsen, G. K. H.; Hammer, B. *J. Chem. Phys.* **2011**, *135*, 084704.
- (38) Henkelman, G.; Uberuaga, B. P.; Jónsson, H. *J. Chem. Phys.* **2000**, *113*, 9901–9904.
- (39) Bredow, T.; Giordano, L.; Cinquini, F.; Pacchioni, G. *Phys. Rev. B* **2004**, *70*, 035419.
- (40) Kiejna, A.; Pabisiaik, T.; Gao, S. W. *J. Phys.: Condens. Matter* **2006**, *18*, 4207–4217.

- (41) Ferrighi, L.; Hammer, B.; Madsen, G. K. H. *J. Am. Chem. Soc.* **2009**, *131*, 10605–10609.
- (42) Vilhelmsen, L. B.; Walton, K. S.; Sholl, D. S. *J. Am. Chem. Soc.* **2012**, *134*, 12807–12816.
- (43) Barrio, L.; Liu, P.; Rodríguez, J. A.; Campos-Martn, J. M.; Fierro, J. L. G. *J. Chem. Phys.* **2006**, *125*, 164715.
- (44) Mavrikakis, M.; Stoltze, P.; Nørskov, J. K.; Mavrikakis, M.; Stoltze, P.; Nørskov, J. K. *Catal. Lett.* **2000**, *64*, 101–106.
- (45) Henkelman, G.; Arnaldsson, A.; Jónsson, H. *Comput. Mater. Sci.* **2006**, *36*, 354–360.
- (46) Lopez, N.; Janssens, T. V. W.; Clausen, B. S.; Xu, Y.; Mavrikakis, M.; Bligaard, T.; Nørskov, J. K. *J. Catal.* **2004**, *223*, 232–235.
- (47) Wang, Y.-G.; Yoon, Y.; Glezakou, V.-A.; Li, J.; Rousseau, R. *J. Am. Chem. Soc.* **2013**, *135*, 10673–10683.
- (48) Wang, J.; Hammer, B. *Phys. Rev. Lett.* **2006**, *97*, 136107.
- (49) Ward, T.; Delannoy, L.; Hahn, R.; Kendell, S.; Pursell, C. J.; Louis, C.; Chandler, B. D. *ACS Catal.* **2013**, *3*, 2644–2653.
- (50) Bamwenda, G. R.; Tsubota, S.; Nakamura, T.; Haruta, M. *Catal. Lett.* **1997**, *44*, 83–87.
- (51) Yoon, B.; Hakkinen, H.; Landman, U.; Worz, A. S.; Antonietti, J.-M.; Abbet, S.; Judai, K.; Heiz, U. *Science* **2005**, *307*, 403–407.
- (52) Kandoi, S.; Greeley, J.; Sanchez-Castillo, M.; Evans, S.; Gokhale, A.; Dumesic, J.; Mavrikakis, M. *Top. Catal.* **2006**, *37*, 17–28.